

Experimental quantum e-commerce

Xiao-Yu Cao,^{1,*} Bing-Hong Li,^{1,*} Yang Wang,^{1,2} Yao Fu,³ Hua-Lei Yin,^{1,†} and Zeng-Bing Chen^{1,‡}

¹*National Laboratory of Solid State Microstructures and School of Physics,*

Collaborative Innovation Center of Advanced Microstructures, Nanjing University, Nanjing 210093, China

²*Henan Key Laboratory of Quantum Information and Cryptography, SSF IEU, Zhengzhou 450001, China*

³*Beijing National Laboratory for Condensed Matter Physics and Institute of Physics,
Chinese Academy of Sciences, Beijing 100190, China*

E-commerce, a type of trading that occurs at a high frequency on the Internet, requires guaranteeing the integrity, authentication and non-repudiation of messages through long distance. As current e-commerce schemes are vulnerable to computational attacks, quantum cryptography, ensuring information-theoretic security against adversary's repudiation and forgery, provides a solution to this problem. However, quantum solutions generally have much lower performance compared to classical ones. Besides, when considering imperfect devices, the performance of quantum schemes exhibits a significant decline. Here, for the first time, we demonstrate the whole e-commerce process of involving the signing of a contract and payment among three parties by proposing a quantum e-commerce scheme, which shows resistance of attacks from imperfect devices. Results show that with a maximum attenuation of 25 dB among participants, our scheme can achieve a signature rate of 0.82 times per second for an agreement size of approximately 0.428 megabit. This proposed scheme presents a promising solution for providing information-theoretic security for e-commerce.

I. INTRODUCTION

Developing algorithms and quantum attacks threaten the security of classic cryptography [1–4]. Since the security of current cryptographic schemes tend to rely on computationally hard mathematical problems [5–8], information-theoretic security against unlimited computational power, has been a hot topic. Quantum mechanics is one of the approaches [9–12]. Quantum key distribution (QKD), which is the most mature application field of quantum technology, offers two remote users unconditionally secure keys [9, 10]. Combined with one-time pad, QKD successfully guarantees the confidentiality of messages.

Secure identification is another important application domain in the realm of the quantum internet [13], which can help guarantee the security during financial transactions. E-commerce, as an indispensable part of daily life, requires identification of the parties and non-repudiation of the contract. A commitment among different participants is required to guarantee the validity of a transaction. The security of classical e-commerce schemes tends to be based on public-key cryptography algorithms [5–8], which is only secure assuming the limited computation power, and there lacks an effective solution to defend against external attacks. Additionally, the presence of dishonest participants may render the contract invalid. Cryptography contains four main information security objectives, confidentiality, integrity, authenticity, and non-repudiation [14]. The integrity, authenticity, and non-repudiation of messages need to be assured in an

e-commerce scheme. The integration of QKD with one-time pad, only promising confidentiality for messages, fails to accomplish this task. Quantum digital signatures (QDS) can provide information-theoretic security for the last three primitives, and thus is suitable for e-commerce scenarios.

QDS was proposed first at 2001 [15]. The original version has many impractical experimental requirements, which made its implementation impossible with available technology. With the development in the next decade, the requirements of swap test and quantum memory are removed [16–18]. Nevertheless, their security analyses were based on secure quantum channels. In 2016, two schemes were proposed independently to solve this problem [19, 20]. Triggered by the two protocols and developments in QKD [21–31], many achievements have been made theoretically [32–38] and experimentally [39–47].

Previous QDS schemes are inefficient when it comes to multi-bit cases and their performances are far from classical solutions. Recently, a new scheme, based on secret sharing, one-time pad, and one-time universal hashing (OTUH), has been proposed [48]. This scheme can sign an arbitrarily long document with a relatively short signature, whose performance outperforms all previous protocols. Furthermore, a variant of this scheme reduces the requirements on keys [49], in which the privacy amplification steps are removed. Besides, security proof of previous schemes tends to be based on assumptions on the ideal devices and there has been a lack of QDS schemes with the ability to solve the loopholes from imperfect devices. To enhance the robustness to imperfect devices, our key generation process (KGP) draws on the development of QKD [21, 50–61]. Four-phase measurement-device-independent (MDI) QKD [61] is secure against possible source flaws and outperforms other protocols in key rate and KGP of our scheme based on this protocol retains its advantage.

* These authors contributed equally.

† hlyin@nju.edu.cn

‡ zbchen@nju.edu.cn

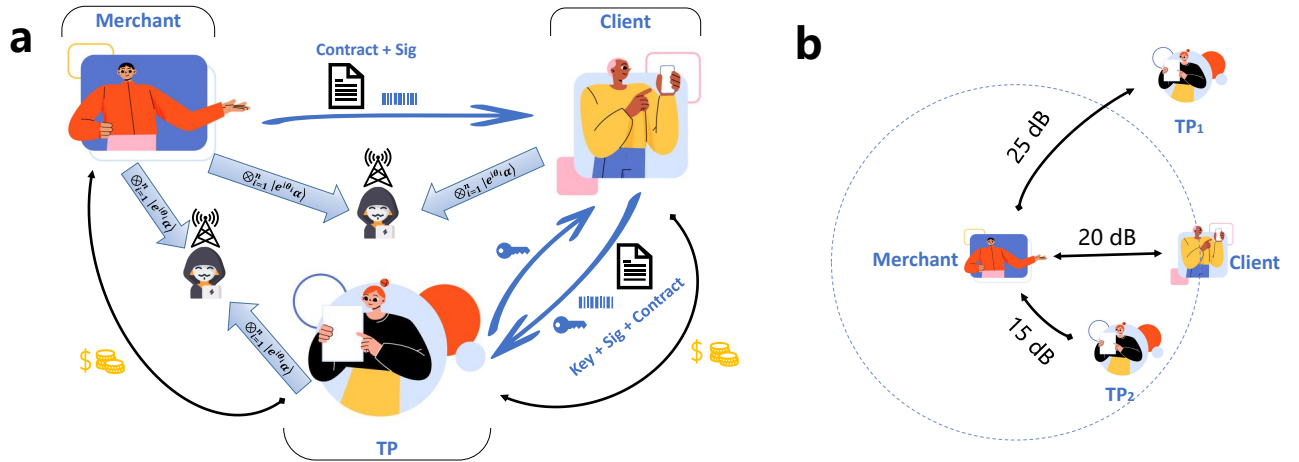


FIG. 1. **a.** Illustration of quantum e-commerce. We consider the three-party scenario where Client buys a product from Merchant. TP is introduced as an arbiter to prevent either Merchant or Client from cheating. Merchant shares two sequences of coherent quantum states with Client and TP, respectively. Merchant then generates the contract with all information of the e-commerce, and obtains a signature through a hash function and keys distilled by his sequences. Thereafter, Merchant sends the contract and signature to Client. Client, if agreeing with the contract, will send the contract, signature and keys distilled by his consequence to TP. TP will then send keys distilled by his own sequence back to Client. Both Client and TP independently verify the signature through their own and received keys by hash functions. Client will pay the money to TP if he verifies the signature. TP will transfer the money to Merchant if he also passes the signature. **b.** A diagram of users in quantum networks. Here we consider a case where the distance between Merchant and Client is fixed and there exists more than one TP.

Here, we present a quantum solution for e-commerce scenarios by proposing an efficient quantum e-commerce scheme based on the ideas mentioned above, which offers security advantages over classical schemes. Motivated by OTUH scheme [48, 49] and four-phase MDI-QKD [61], our scheme is able to sign multi-bit documents with high efficiency while mitigating the impact of imperfect devices, and thus improves the overall security and practicality of the scheme. The signature rate is only limited by the minimum key rate of KGP between different participants and merchant. Our experimental implementation on a multi-user quantum network successfully signs a 0.428-megabit (Mb) agreement 0.82 times per second with a maximum attenuation of 25 dB between a participant and merchant. We also characterize the imperfections of the sources experimentally. Our work contributes to the further development of e-commerce in the quantum era by providing a practical and efficient solution with enhanced security.

section

II. PROTOCOL DESCRIPTION

In a classical e-commerce scenario, a third party (TP) is always required and assumed as trusted. Thus, only those with high authority can be a TP, leading to a requirement of centralized systems. Here, we propose a three-party quantum e-commerce protocol with no as-

sumptions on TP. In the protocol we describe a scenario where Client buys a product from Merchant through a network, and TP is an arbiter to help finish the whole process successfully. In the network with numerous nodes, TP can be an arbitrary party since there are no assumptions on it. A decentralized system can be realized based on our proposed three-party protocol. A schematic of the quantum e-commerce protocol is illustrated below and shown in Fig. 1a.

(i) **Distribution:** Merchant prepares two sequences of coherent states $|X_1\rangle$ and $|X_2\rangle$, and keeps the phase of every state. Client also prepares a sequence $|Y_1\rangle$ and the TP prepares $|Y_2\rangle$. Through a Merchant-Client quantum channel, Merchant sends $|X_1\rangle$ and Client sends $|Y_1\rangle$ to an untrusted intermediate Eve who performs interference measurements on the received pulses with a 50:50 beam splitter (BS) and two single-photon detectors, and announces the detection results m_1 . Likewise, $|X_2\rangle$ and $|Y_2\rangle$ are sent to an untrusted intermediate through the Client-TP channel, and the detection results m_2 are announced.

(ii) **Signature:** To sign a contract, Merchant distills a $3n$ -bit key k_1^M from $|X_1\rangle$ and m_1 . He will select states in $|X_1\rangle$ that successfully intervene with that in $|Y_1\rangle$ according to the detection results m_1 . He also communicates with Client through an authenticated channel to sift the keys, and finally chooses a $3n$ -bit substring to form k_1^M . Likewise, Merchant distills a $3n$ -bit key k_2^M from $|X_2\rangle$ and m_2 .

The keys $k_1^M \xleftarrow{m_1} |X_1\rangle$ and $k_2^M \xleftarrow{m_2} |X_2\rangle$ are used to generate the signature of the contract. The signature is generated through a universal hash function $Sig = Hash(C, k_1^M \oplus k_2^M)$, with a length of n -bit, where C is the contract containing all details including timestamp, the identity of Merchant and Client. The function $Hash$ is composed of a linear feedback shift register (LFSR) Toeplitz functions. Details are shown in Methods.

(iii) Transference: Merchant sends the contract and signature $\{C, Sig\}$ to Client. If Client agrees with the contract, he distills a key $k_1^C \xleftarrow{m_1} |Y_1\rangle$, following the rules same as that of Merchant. He then send $\{C, Sig, k_1^C\}$ to TP.

TP also obtains $k_2^T \xleftarrow{m_2} |Y_2\rangle$. He will send his key k_2^T to Client after he receives $\{C, Sig, k_1^C\}$.

(iv) Verification and payment: Both Client and TP independently verify the signature by calculating $Hash(C, k_1^C \oplus k_2^T)$ and comparing the result with Sig . If the result is identical to Sig , the signature is successfully passed. Client will pay the money to TP if he verifies the signature. TP, after receiving the payment, will transfer the money to Merchant if he passes the signature. Otherwise, he will return the money to Client and announce that the contract is aborted.

In the distribution step, the participants essentially share correlated and secret quantum states. The secrecy of the interpreted keys, together with one-time hashing, protects the security of the program against Client's tampering attacks. The transference step guarantees that Client and TP obtain the same final keys. Merchant's repudiation attacks are prevented by TP because TP will always make the correct judgment if Client is honest.

III. SECURITY ANALYSIS

The proposed scheme is a three-party protocol without strong assumptions on TP. In other words, the three parties have equal status and the final decision is made by voting principle if disagreement happens. It must be assumed that at most one party can be malicious. Otherwise, malicious parties can cooperate to finish the attack by controlling the voting result. In security analysis, we consider four cases: honest abort, Merchant's repudiation attack, Client's forgery attack, and TP's forgery attack.

Robustness. If Merchant and Client (or TP) share different key bits after the distribution stage, the protocol will be aborted even if the users are all honest. That is, an honest run abortion occurs. In the protocol, Merchant and Client (TP) perform error correction on their final keys, with a failure probability of no more than ϵ_{EC} . The correctness of classical information transference is protected by classical information technology such as authenticated channels, whose failure probability is set as no more than ϵ' . The probability that Merchant and Client share different final key is no more than $\epsilon_{EC} + \epsilon'$, and the same for Merchant and TP. Thus the robustness

bound is $\epsilon_{rob} = 2\epsilon_{EC} + 2\epsilon'$. Since ϵ' is a parameter of classical communication, we assume it as $\epsilon' = 10^{-10}$ in the simulation.

Repudiation. In a repudiation attack, Merchant attempts to let Client accept the contract while TP rejects it so that he can successfully deny the contract. For Merchant's repudiation attacks, Client and TP are both honest and symmetric and thus hold the same new key strings. They will make the same decision for the same contract and signature. Repudiation attacks succeed only when errors occur in one of the transference steps. The repudiation bound is $\epsilon_{rep} = 2\epsilon'$.

Forgery. In Client's forgery attack, Client will tamper the contract and attempts to let TP accept the tampered contract forwarded to him. According to our protocol, TP accepts the contract if and only if TP obtains the same result as Sig through one-time hash functions. Actually, this is the same as an authentication scenario where Client is the attacker attempting to forge the information sent from Merchant to TP. TP also has the motivation to perform forgery attack. He may attempt to intercept the contract C and tamper the information of price in it. If Client agrees with the tampered (higher) price, TP can earn the price difference secretly. This is the same as an authentication scenario where TP is the attacker attempting to forge the information sent from Merchant to Client. Thus, Client and TP's forgery attacks are equivalent, and we only analyze Client's in the following.

In the hash function $Hash(C, k_1^M \oplus k_2^M)$, $k_1^M \oplus k_2^M$ is actually divided into three n -bit substrings. Here we rewrite it as $k_1^M \oplus k_2^M = (x_2, x_3, x_4)$ to keep consistent with that in Methods. Define $\mathcal{H}_n = H_{\min}(\mathbb{X}|\mathbb{B})_\rho$ as the min-entropy of \mathbb{X} and \mathbb{B} , where $\mathbb{X} \in \{x_2, x_3, x_4\}$ and \mathbb{B} represents Client's guessing for \mathbb{X} . We can estimate \mathcal{H}_n through parameters in the distribution stage. More details are shown in Methods. Then we can bound the probability that the attacker correctly guesses \mathbb{X} when using an optimal strategy according to the definition of min-entropy [62],

$$P_{\text{guess}}(\mathbb{X}|\mathbb{B}) = 2^{-H_{\min}(\mathbb{X}|\mathbb{B})_\rho} = 2^{-\mathcal{H}_n}. \quad (1)$$

Thereafter, we can obtain the failure probability of an authentication scenario where Client is the attacker attempting to forge the information sent from Merchant to TP, which is equivalent to the fogery bound in our scheme. [49]

$$\epsilon_{\text{for}} = m \cdot 2^{1-\mathcal{H}_n}. \quad (2)$$

The number of malicious parties is no more than one, i.e., at most one of the above cases happens. Thus, the total security bound, i.e., the maximum failure probability of the protocol, is $\epsilon_{\text{tot}} = \max\{\epsilon_{rob}, \epsilon_{rep}, \epsilon_{for}\}$.

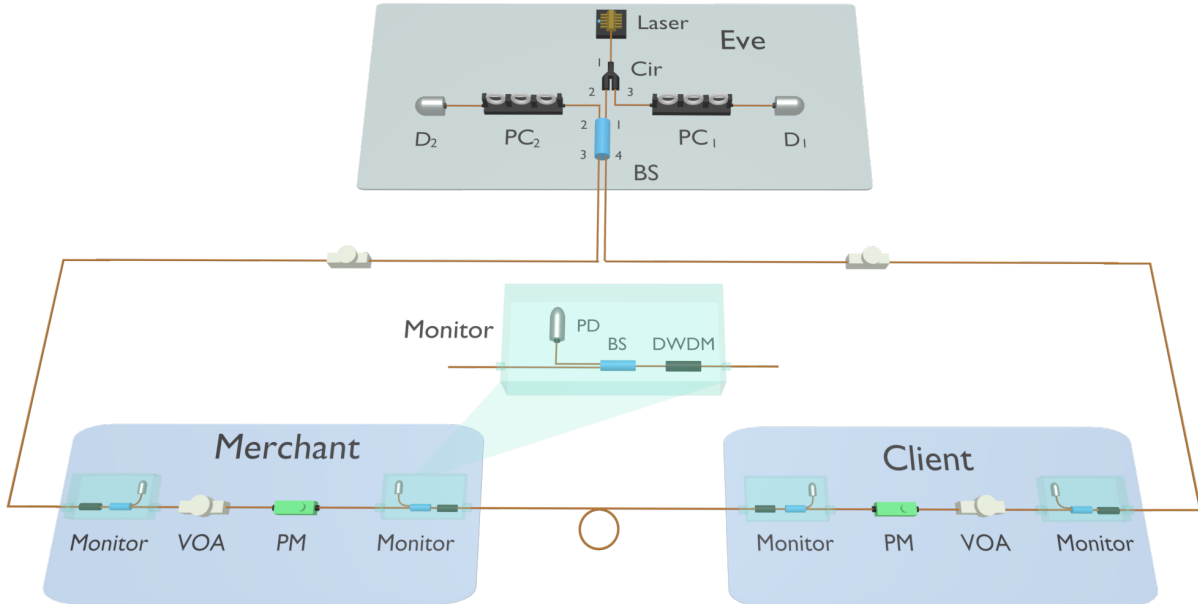


FIG. 2. **Experimental setup of KGP between Merchant and Client.** The pulses are generated by a pulsed laser with an extinction ratio of over 30 dB and then split into two pulse sequences with a 50:50 beam splitter (BS). The pulses entering the loop are subjected to modulation by the phase modulator (PM) operated by either Merchant or Client. Monitor module consists of a dense wavelength division multiplexing (DWDM), a BS and a photon detector (PD). After phase modulation, these two pulses interfere in the Eve’s BS and are detected by two superconducting nanowire single-photon detectors D_1 and D_2 . One of the pulse sequences is from the port 2 to the port 3 of the circulator (Cir), and then detected by D_1 . Variable optical attenuators (VOA) are used to adjust the intensity of sending pulses and simulate the channel loss. Polarization controllers (PCs) are utilized to control the polarization of the pulses.

IV. EXPERIMENTAL DEMONSTRATION

We provide a proof-of-principle demonstration of the entire process here. The scenario considered involves transactional activities between Client and Merchant, with the requirement of a TP to facilitate the purchase transaction. The network consists of two TPs, denoted as TP_1 and TP_2 . As illustrated in Fig. 1b, the channel loss between the Merchant and Client is a constant value of 20 dB, whereas the channel loss between the Merchant and TP_1 is 15 dB, and that between the Merchant and TP_2 is 25 dB. As there are no assumptions on TP, in practical networks there can be multiple TPs present.

The signature process requires key generation and distribution between Merchant-Client and Merchant-TP, which is facilitated by KGP. In this work, we consider the KGP based on four-phase MDI-QKD [61], which remains robust against imperfect devices. Details about four-phase MDI-KGP can be seen in Methods. The system’s source flaws are characterized before KGP, including optical power fluctuation, extinction ratio of polarization, phase shift, and pattern effects, and are quantified through a detailed measurement process outlined in Supplementary Information. The keys used for signature

are generated in a plug-and-play system [24, 61], and the global phase of pulses is stabilized by a Sagnac loop. We take KGP between Merchant and Client as an example.

As depicted in Fig. 2, optical pulses modulated by users are generated by an untrusted third party, Eve, and the pulses are separated into two identical pulses. Merchant (Client) modulates the clockwise (anticlockwise) pulses. Merchant (Client) randomly chooses the X basis with a probability of $p_x = 90\%$ and the Y basis with a probability of $p_y = 10\%$ and encodes the pulses according to the values of logic bits. After appropriate attenuation, quantum states $|e^{i\theta}\alpha\rangle$ are successfully generated, where θ is the phase modulated by two participants and the intensity of the pulse is $|\alpha|^2$. The use of the Sagnac loop has helped to solve the problem of phase locking, but it has also introduced security concerns due to the possibility of pulses generated by a third party. Therefore, a monitoring module has been added to the participant side to filter and monitor the intensity of the incident pulses, aiming to enhance the security of the system. Due to resource limitations, we did not include dense wavelength multiplexings in the system, and instead opted to replace the photon detectors with power meters during implementation. We would like to emphasize that these modifications have little impact on the results.

TABLE I. Four parameters related to the imperfection of realistic sources. The parameters included the optical power fluctuation ξ , phase shift δ , the extinction ratio of polarization $\tan\theta$, pattern effect ψ and THAs μ . Note that THAs cannot be quantified during our implementation and we set it to a typical value 10^{-7} [64].

	ξ	δ	$\tan\theta$	ψ
Merchant - TP ₁	0.79%	0.038	$10^{-2.92}$	5.58×10^{-3}
Merchant - Client	0.69%	0.035	10^{-3}	5.89×10^{-3}
Merchant - TP ₂	0.62%	0.035	$10^{-2.98}$	6.91×10^{-3}

Two variable optical attenuators (VOA) are placed between Merchant and Eve, and between Client and Eve, respectively, in order to simulate the attenuation caused by the communication channel. After interference at Eve's BS, the results are detected by D₁ and D₂. The time window is selected based on detection data, whose length is 2 ns. The detection efficiency η_{d_1} of D₁ is 84.4% and the dark count rate p_{d_1} is 4.4 Hz. For D₂, the detection efficiency η_{d_2} is 85.5% and the dark count rate p_{d_2} is 2.5 Hz. After error correction, Merchant gets k_1^M and Client gets k_1^C . The same is for Merchant and TP, where Merchant gets k_2^M and TP gets k_2^T .

For demonstration, we sign a file with a size of 0.428 Mb, which is approximately the size of Amazon Web Services Customer Agreement (428072 bits) [63]. Merchant generates the signature *Sig* by $Hash(C, k_1^M \oplus k_2^M)$ and sends it and contract to Client. If Client agrees with the contract, she (or he) will forward $\{Sig, k_1^C\}$ to TP. LFSR-based Toeplitz function is used and a detailed description can be seen in Methods. Upon receiving the signature and contract, TP sends his key k_2^T to Client. Then, Client and TP verify the signature independently by comparing the result of $Hash(C, k_1^C \oplus k_2^T)$ to *Sig*. If the signature is successfully verified by both parties, Client will send money to TP, who will in turn pay the Merchant. Otherwise, the contract will be aborted.

V. EXPERIMENTAL RESULTS

Before KGP, we need to characterize the relative parameters corresponding to source flaws of this system. Similar to Ref. [61], we denote optical power fluctuation, phase shift, extinction ratio of polarization, and pattern effect ξ , δ , $\tan\theta$ and ψ , respectively. Note that although trojan horse attacks (THA) can be resisted in the schemes of two independent users, it cannot be resisted in the plug-and-play system and we set the parameter of THAs to $\mu = 10^{-7}$ [64]. Results are shown in Table I.

The channel loss between Merchant and Client is fixed at 20 dB. The channel loss between Merchant and TP is set to two scenarios: 15 dB and 25 dB. During KGP, the system frequency is 100 MHz and for each pair of participants, the system operates for 100 seconds. Signature

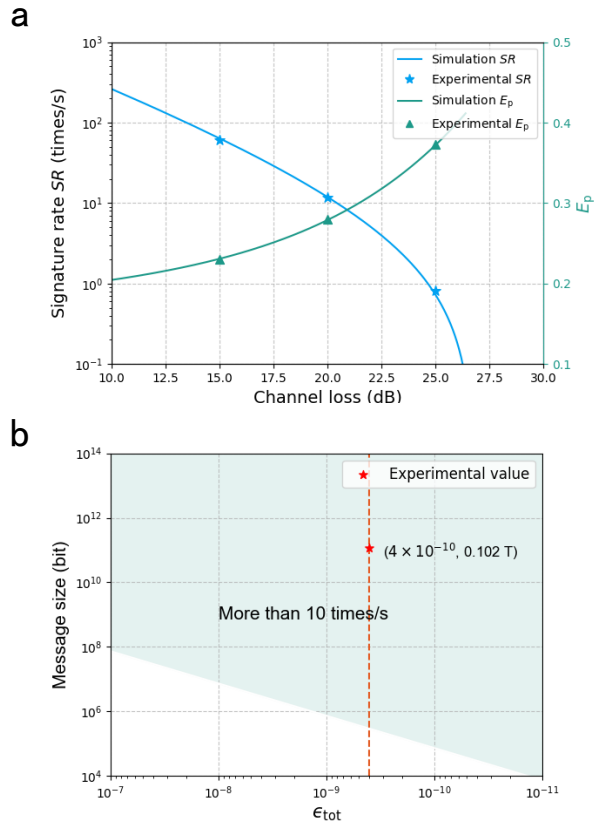


FIG. 3. **Results of demonstration.** **a.** Signature rate R under different losses. The total number of pulses sent is 10^{10} . **b.** The relationship between security level and different sizes of files with a key of the same length. The boundary line represents the scenario where the generation rate of keys per second is sufficient to sign a 0.428-Mb file at a security level of 5×10^{-10} ten times with the same error rate under a 20dB attenuation. In our implementation, a 0.428-Mb document can be signed 11.83 times while maintaining the 5×10^{-10} security level. Furthermore, with the keys generated within one second, a document of 0.102-terabit (Tb) can be signed ten times at a security level of 4×10^{-10} ($\epsilon_{\text{rob}} = 4 \times 10^{-10}$).

rate under different losses is shown in Fig. 3a. As a proof-of-principle demonstration, we conducted KGP among different participants within a system. Sagnac loop in the system is used for stabilizing the global phase between two participants and the bit error rate can be kept around 0.10%. Detailed data is shown in Table II. Due to the consideration of imperfect sources, the increasing rate of phase error rate is higher compared to protocols of the same type. For 0.428-Mb size document, if TP₁ is chosen as the third party, the key formed within 100 seconds can be used for signing 1183 times while if TP₂ is chosen, the number of signature times is 82. As shown in Fig. 3b, for the same key generation rate, a higher security level implies a smaller signing file size. There exists a tradeoff between the security level and the size of the

signed file. Besides, a minor increase in the signature key length can result in a significant increase in the size of the signed files, which demonstrates its ability to sign multi-bit files. The signature rates of the three-party system are limited by the minimum key rate of KGP among the three parties. In practical scenarios, participants can store the keys in advance to reduce the time required for signature generation.

VI. DISCUSSION

We demonstrate the whole process of quantum e-commerce, which guarantees the one-time of purchase with information-theoretic security. As the length of the signature increases, the probability of cheating approaches zero. The QDS scheme can complete multiple contract signatures within one second, further narrowing the gap between quantum and classical schemes.

We have considered a real-world scenario where Merchant and Client need to carry out a transaction and establish a consensus to complete it. TP is introduced to finish the process. Unlike the classical setup where third parties are usually considered trustworthy by default, there are no assumptions on TP. We take the Amazon Web Services Customer Agreement [63] with the size of 428072 bits and demonstrate the underlying principles of the process. Note that the size of the contract affects the final performance instead of the content. The signature rates of the system are limited by the minimum key rate of KGP among the three parties. Consequently, the signature rate of a 0.428-Mb document can reach 11.83 times per second when choosing TP₁ and 0.82 times per second with TP₂.

The proposed quantum e-commerce scheme, employing QDS, offers a solution for ensuring message authenticity and integrity in the presence of imperfect keys and devices. The elimination of privacy amplification reduces the computational resources and running time of post-processing. Furthermore, a thorough experimental characterization of source flaws in the scheme is conducted. This feature distinguishes our scheme as a practical solution for addressing the issue of imperfect keys and devices in the field of quantum communication. The proposed scheme also demonstrates robustness against security levels and finite-size effects, making it highly compatible with future quantum networks and suitable for a variety of applications.

In summary, the proposed scheme can accomplish the task of e-commerce with practical devices and outperforms other quantum protocols. We have validated the effectiveness of our scheme through the demonstration of an e-commerce scenario, involving a transaction between Merchant and Client that required a consensus to complete. It presents a promising approach to ensuring message authenticity and integrity in the presence of imperfect keys and devices.

ACKNOWLEDGMENTS

This study was supported by the National Natural Science Foundation of China (No. 12274223), the Natural Science Foundation of Jiangsu Province (No. BK20211145), the Fundamental Research Funds for the Central Universities (No. 020414380182), and the Program for Innovative Talents and Entrepreneurs in Jiangsu (No. JSSCRC2021484).

Appendix A: Four-phase MDI-KGP between Merchant and Client

During implementation, Merchant, Client, and TP send their quantum states to the intermediates who perform interference measurements on the received pulses and announce the outcomes. These three parties will later distill their keys through their quantum states and measurement results announced by the intermediates. This process, in detail, is equivalent to four-phase MDI-KGP between Merchant and Client, and between Merchant and TP.

Here, we give a brief introduction to four-phase MDI-KGP in Merchant-Client channel to show the details of steps (i)-(iii) in protocol description.

(i) *Preparation.* Both of Merchant and Client randomly choose the X and Y bases with probabilities p_x ($0 < p_x < 1$) and $p_y = 1 - p_x$, respectively. For X basis, Merchant encodes a coherent state $|e^{ik_x^M \pi \alpha}\rangle$ with the logic bit $k_x^M \in \{0, 1\}$, where $|\alpha|^2$ is the intensity of the optical pulse. For Y basis, Merchant prepares a coherent state $|e^{i(k_y^M + \frac{1}{2})\pi \alpha}\rangle$ according to random logic bit $k_y^M \in \{0, 1\}$. Client prepares his own state $|e^{ik_x^C \pi \alpha}\rangle$ or $|e^{i(k_y^C + \frac{1}{2})\pi \alpha}\rangle$ according to the same rule. Then, Merchant and Client send their optical pulses to an untrusted relay, Eve, through insecure quantum channels.

(ii) *Measurement.* Eve performs interference measurements on the received pulses with a 50: 50 BS and two single-photon detectors, denoted as D₁ and D₂, and records the detection results. Those where one and only one detector clicks are defined as an effective measurement.

(iii) *Sifting.* Merchant and Client repeat Steps (i)-(ii) for N times. $|X_1\rangle = \otimes_{i=1}^N |i\rangle$, $|i\rangle \in \{|e^{ik_x^M \pi \alpha}\rangle, |e^{i(k_y^M + \frac{1}{2})\pi \alpha}\rangle\}$ is all Merchant's states in direct product state. Likewise, $|Y_1\rangle = \otimes_{j=1}^N |j\rangle$, $|j\rangle \in \{|e^{ik_x^C \pi \alpha}\rangle, |e^{i(k_y^C + \frac{1}{2})\pi \alpha}\rangle\}$ is all Client's states in direct product state. Eve announces the location of all effective measurements and which detector (D₁ or D₂) clicks. For every effective measurement announced by Eve, if D₂ clicks, Client will flip his corresponding logic bit (k_x^C or k_y^C). Merchant and Client will only keep their logical bits of effective measurements and discard other bits. Then they disclose their basis choices for effective measurements through authenticated classical channels, and

TABLE II. Summary of experimental data. We tested the signature rate between different users. The number of total pulses sent is $N = 10^{10}$. The intensity of pulses μ , the experimental bit error rate under X basis and Y basis E_b^x and E_b^y , the total number of leaked bits of information during error correction leak_{EC} and signature rate SR are included in the table.

Participants	μ	E_b^x	E_b^y	E_p	leak_{EC}	SR
Merchant - TP ₁	7.40×10^{-3}	0.10%	0.07%	23.0%	185875	60.10
Merchant - Client	4.20×10^{-3}	0.10%	0.06%	28.0%	59209	11.83
Merchant - TP ₂	2.30×10^{-3}	0.10%	0.10%	37.3%	18129	0.82

further classify their key bits with basis information.

(iv) *Parameter estimation.* Merchant and Client publicize all their bits in the Y basis to calculate the bit error rate E_b^y , and also obtain the number of counts n_x and n_y under X and Y bases, respectively.

(v) *Key distillation.* Merchant and Client perform error correction on the remaining keys under the X basis with ε_{cor} -correctness to obtain the final keys.

Merchant then randomly disturbs the orders of his final key string, and publicizes the new order to Client through authenticated channels. Subsequently, Client change the orders of his key strings according to the order announced by Merchant. Finally, Merchant and Client divide their final keys into $3n$ -bit strings, each of which is used to sign a message. Each of k_1^M , k_2^M , k_1^C , and k_2^T is one string.

Appendix B: LFSR-based Toeplitz hash functions

In the protocol, we utilize universal hash functions to generate the signature. Concretely, we choose LFSR-based Toeplitz hash function $\text{Hash}(C, k)$. To show details of the function, we rewrite it as $\text{Hash}(C, k) = \text{Hash}(x_1, x_2, x_3, x_4)$, where $C = x_1 \in \{0, 1\}^{|C|}$ corresponds to the contract and $k = (x_2, x_3, x_4) \in \{0, 1\}^{3n}$ corresponds to keys in step (ii) of protocol. The lengths of x_2, x_3, x_4 are all n -bit. Denote the length of x_1 as m , i.e., $|C| = m$. Then

$$\text{Hash}(x_1, x_2, x_3, x_4) = H_{nm} \cdot x_1 \oplus x_4, \quad (\text{B1})$$

where $H_{nm} = f(x_2, x_3)$ is a LFSR-based Toeplitz matrix determined by x_2 and x_3 . The random string x_2 maps a random irreducible polynomial $p(x) = x^n + p_{n-1}x^{n-1} + \dots + p_1x + p_0$ in $\text{GF}(2)$ of order n that decide the structure of LFSR. Another random string $x_3 = (a_n, a_{n-1}, \dots, a_2, a_1)^T$, $a_i \in \{0, 1\}$ is the initial state. LFSR will expand the initial state into a matrix H_{nm} with n rows and m columns. The structure of LFSR can be represented as an $n \times n$ matrix

$$W = \begin{pmatrix} p_{n-1} & p_{n-2} & \dots & p_1 & p_0 \\ 1 & 0 & \dots & 0 & 0 \\ 0 & 1 & \dots & 0 & 0 \\ \dots & \dots & \dots & \dots & \dots \\ 0 & 0 & \dots & 1 & 0 \end{pmatrix}. \quad (\text{B2})$$

The structure of LFSR-based Toeplitz matrix can be represented as $H_{nm} = (x_3, Wx_3, \dots, W^{m-1}x_3)$ [65].

Appendix C: Calculation details

Here, we give an introduction to the calculation details of KGP used in the scheme. According to the Ref. [61], only key bits under the X basis are used to form secure key bits. Since the privacy amplification step is removed in our scheme, the total unknown information of the l -bit string such as x_i , $i \in \{2, 3, 4\}$ in LFSR-based Toeplitz hash functions considering finite-key effect is given by

$$\mathcal{H}_n = l \cdot \left[1 - H(\bar{E}_p^l) - \frac{1}{n_x} \text{leak}_{\text{EC}} - \frac{1}{n_x} \log_2 \frac{2}{\epsilon_{\text{EC}}} \right], \quad (\text{C1})$$

where n_x is the total counts under the X basis. \bar{E}_p^n is the upper bound of the phase error rate of all counts in an n -bit string. $\text{leak}_{\text{EC}} = n_x fH(E_b^x)$ is the number of leaked bits of information during the error correction, where f is the error correction efficiency and E_b^x is the bit error rate in X basis. $H(x) = -x \log_2 x - (1-x) \log_2 (1-x)$ is the binary Shannon entropy function. \bar{E}_p^l can be given by

$$\bar{E}_p^l = \bar{E}_p + \gamma^U(l, n_x - n, E_p, \epsilon), \quad (\text{C2})$$

where $\gamma^U(l, k, \lambda, \epsilon) = \frac{\frac{(1-2\lambda)AG}{l+k} + \sqrt{\frac{A^2G^2}{(l+k)^2} + 4\lambda(1-\lambda)G}}{2 + 2\frac{A^2G}{(l+k)^2}}$ represents the statistical fluctuation of the random sampling without replacement, with $A = \max\{l, k\}$ and $G = \frac{l+k}{lk} \ln \frac{l+k}{2\pi lk \lambda(1-\lambda)\epsilon^2}$ [66], and \bar{E}_p is the upper bound of phase error rate. E_p is bounded by [61, 67]

$$1 - 2\Delta \leq \sqrt{E_b^y E_p} + \sqrt{(1 - E_b^y)(1 - E_p)}, \quad (\text{C3})$$

where E_b^y is the quantum bit error rate in the Y basis and Δ quantifies the imbalance of Alice's and Bob's quantum coins based on their basis choices. In the symmetric scenario, the relation between Δ and fidelity can be simplified as $1 - 2Q\Delta = \text{Max}_{\delta_\theta, \delta_X, \delta_Y} \text{Re}(e^{i\delta_\theta} \langle \Psi_{Y, \delta_Y} | \Psi_{X, \delta_X} \rangle) | \langle \Psi_Y | \Psi_X \rangle |$ [68],

where Q is the total gain and δ_θ , δ_X , and δ_Y are free variables, the values of which range from 0 to 2π . $|\Psi_{Z,\delta_Z}\rangle = (|0_Z\rangle|\Psi_{0Z}\rangle + |1_Z\rangle|\Psi_{1Z}\rangle)/\sqrt{2}$. $|\Psi_{iZ}\rangle$ means the state is prepared under the Z basis ($Z \in \{X, Y\}$) with the bit value i ($i \in \{1, 0\}$). The fidelity with imperfect sources can be expressed as

$$\begin{aligned} \langle \Psi_X | \Psi_Y \rangle = & \frac{1}{4}(1 - \epsilon)e^{-\mu} \cos^2 \theta [(1 - i) \langle \alpha' | i e^{i\delta} \alpha' \rangle \\ & + (1 - i) \langle -e^{i\delta} \alpha' | -i e^{i\delta} \alpha' \rangle \\ & + (1 + i) \langle \alpha' | -i e^{i\delta} \alpha' \rangle \\ & + (1 + i) \langle -e^{i\delta} \alpha' | i e^{i\delta} \alpha' \rangle], \end{aligned} \quad (\text{C4})$$

where ϵ , μ , θ , and δ represent pulse correlations, THAs, side channels in the polarization space, and phase shift, respectively. Note that α' is the actual intensity of pulses. According to the formulas above, we can get Δ .

Considering the finite key effect, we use the bound of the concentration inequality [61, 69] to derive the upper bound of E_p . The inequality is

$$\Lambda_n \leq \sum_{u=1}^n \Pr(\xi_u = 1 | \xi_1, \dots, \xi_{u-1}) + \Delta_n, \quad (\text{C5})$$

where ξ_1, \dots, ξ_n is a sequence of Bernoulli random variables and $\Lambda_n = \sum_{u=1}^n \xi_u$. $\Delta_n = \sqrt{\frac{1}{2} n \ln \epsilon_F^{-1}}$, where ϵ_F is the failure probability. $m_y = n_y E_b^y$ is the number of bit errors in the Y basis and the upper bound of the expectation value of $m_y^* = m_y + \Delta_{n_y}$. Thus, $E_b^{y*} = m_y^*/n_y$ and then E_p^* can be calculated according to Eq. C3. So $m_p^* = n_x E_p^*$. Then estimate the upper bound \bar{m}_x through the concentration inequality. \bar{E}_p can be naturally calculated with $\bar{E}_p = \bar{m}_p/n_x$. We set all failure probabilities $\epsilon_{EC} = \bar{\epsilon} = \epsilon_F = 10^{-10}$ during calculation. Parameter n is optimized with the constrain that $\epsilon_{\text{tot}} \leq 5 \times 10^{-10}$.

Appendix D: Error correction algorithm

In our implementation, the error correction algorithm is used to ensure that the keys generated by both parties through the KGP process are completely identical and the algorithm we use is Cascade algorithm [70]. The block size for each error correction is set to 1M and the size of the remaining keys is smaller than 1M and these keys are corrected together. The detailed process is presented as follows:

(i) Alice and Bob randomly permute the original keys based on a pre-agreed random sequence and record the permutation information.

(ii) The permuted keys are divided into different segments of a fixed length. We set the length 600.

(iii) The parity check codes for each segment are computed, and both parties compare them over a publicly authenticated channel.

(iv) For segments with consistent parity check codes, no further processing is performed. For segments with different codes, error correction is performed using binary search.

(v) When the iteration number is greater than 1, based on the recorded random permutation information from the previous round, the position of the key belonging to the error bit can be identified. Since in the previous round, all segments have the same parity check code, indicating either no errors or an even number of errors, if an error bit is discovered in this round, another error bit can be found. Another error bit is found using a binary search algorithm. This process continues until no further error bits can be found.

(vi) The above steps are repeated until the parity check codes for all segments are completely identical.

During implementation, we do not aim for optimal error correction performance, and the number of iterations is limited to a maximum of three. The error correction efficiency f is about 1.13 during our implementation.

-
- [1] P. W. Shor, Polynomial-time algorithms for prime factorization and discrete logarithms on a quantum computer, *SIAM Journal on Computing* **41**, 303 (1999).
- [2] E. Martin-Lopez, A. Laing, T. Lawson, R. Alvarez, X.-Q. Zhou, and J. L. O'Brien, Experimental realization of shor's quantum factoring algorithm using qubit recycling, *Nat. Photonics* **6**, 773 (2012).
- [3] F. Boudot, P. Gaudry, A. Guillevic, N. Heninger, E. Thomé, and P. Zimmermann, Comparing the difficulty of factorization and discrete logarithm: a 240-digit experiment, in *Advances in Cryptology-CRYPTO 2020* (Springer, 2020) pp. 62–91.
- [4] É. Gouzien and N. Sangouard, Factoring 2048-bit rsa integers in 177 days with 13 436 qubits and a multimode memory, *Phys. Rev. Lett.* **127**, 140503 (2021).
- [5] R. L. Rivest, A. Shamir, and L. Adleman, A method for obtaining digital signatures and public-key cryptosystems, *Commun. ACM* **21** (1978).
- [6] R. A. DeMillo, *Foundations of secure computation*, Tech. Rep. (Georgia Institute of Technology, 1978).
- [7] T. Elgamal, A public key cryptosystem and a signature scheme based on discrete logarithms, *IEEE Trans. Inf. Theory* **31**, 469 (1985).
- [8] J. H. Silverman and J. T. Tate, *Rational points on elliptic curves* (Springer, 1992).
- [9] C. H. Bennett and G. Brassard, Quantum cryptography: Public key distribution and coin tossing, *Theor. Comput. Sci.* **560**, 7 (2014).
- [10] A. K. Ekert, Quantum cryptography based on bell's theorem, *Phys. Rev. Lett.* **67**, 661 (1991).
- [11] F. Xu, X. Ma, Q. Zhang, H.-K. Lo, and J.-W. Pan, Secure quantum key distribution with realistic devices, *Rev. Mod. Phys.* **92**, 025002 (2020).
- [12] P. Schiаны, J. Kalb, E. Sztatecsny, M.-C. Roehsner, T. Guggemos, A. Trenti, M. Bozzio, and P. Walther, Demonstration of quantum-digital payments, *Nat. Com-*

- muni. **14**, 3849 (2023).
- [13] S. Wehner, D. Elkouss, and R. Hanson, Quantum internet: A vision for the road ahead, *Science* **362**, eaam9288 (2018).
- [14] A. J. Menezes, P. C. Van Oorschot, and S. A. Vanstone, *Handbook of applied cryptography* (CRC press, 2018).
- [15] D. Gottesman and I. Chuang, Quantum digital signatures, arXiv preprint quant-ph/0105032 (2001).
- [16] P. J. Clarke, R. J. Collins, V. Dunjko, E. Andersson, J. Jeffers, and G. S. Buller, Experimental demonstration of quantum digital signatures using phase-encoded coherent states of light, *Nat. Commun.* **3**, 1174 (2012).
- [17] V. Dunjko, P. Wallden, and E. Andersson, Quantum digital signatures without quantum memory, *Phys. Rev. Lett.* **112**, 040502 (2014).
- [18] R. J. Collins, R. J. Donaldson, V. Dunjko, P. Wallden, P. J. Clarke, E. Andersson, J. Jeffers, and G. S. Buller, Realization of quantum digital signatures without the requirement of quantum memory, *Phys. Rev. Lett.* **113**, 040502 (2014).
- [19] H.-L. Yin, Y. Fu, and Z.-B. Chen, Practical quantum digital signature, *Phys. Rev. A* **93**, 032316 (2016).
- [20] R. Amiri, P. Wallden, A. Kent, and E. Andersson, Secure quantum signatures using insecure quantum channels, *Phys. Rev. A* **93**, 032325 (2016).
- [21] H.-K. Lo, M. Curty, and B. Qi, Measurement-device-independent quantum key distribution, *Phys. Rev. Lett.* **108**, 130503 (2012).
- [22] H.-L. Yin, T.-Y. Chen, Z.-W. Yu, H. Liu, L.-X. You, Y.-H. Zhou, S.-J. Chen, Y. Mao, M.-Q. Huang, W.-J. Zhang, H. Chen, M. J. Li, D. Nolan, F. Zhou, X. Jiang, Z. Wang, Q. Zhang, X.-B. Wang, and J.-W. Pan, Measurement-device-independent quantum key distribution over a 404 km optical fiber, *Phys. Rev. Lett.* **117**, 190501 (2016).
- [23] M. Lucamarini, Z. L. Yuan, J. F. Dynes, and A. J. Shields, Overcoming the rate–distance limit of quantum key distribution without quantum repeaters, *Nature* **557**, 400 (2018).
- [24] X. Zhong, J. Hu, M. Curty, L. Qian, and H.-K. Lo, Proof-of-principle experimental demonstration of twin-field type quantum key distribution, *Phys. Rev. Lett.* **123**, 100506 (2019).
- [25] J.-P. Chen, C. Zhang, Y. Liu, C. Jiang, W.-J. Zhang, Z.-Y. Han, S.-Z. Ma, X.-L. Hu, Y.-H. Li, H. Liu, *et al.*, Twin-field quantum key distribution over a 511 km optical fibre linking two distant metropolitan areas, *Nat. Photonics* **15**, 570 (2021).
- [26] S. Wang, Z.-Q. Yin, D.-Y. He, W. Chen, R.-Q. Wang, P. Ye, Y. Zhou, G.-J. Fan-Yuan, F.-X. Wang, Y.-G. Zhu, *et al.*, Twin-field quantum key distribution over 830-km fibre, *Nat. Photonics* **16**, 154 (2022).
- [27] L. Zhou, J. Lin, Y. Jing, and Z. Yuan, Twin-field quantum key distribution without optical frequency dissemination, *Nat. Commun.* **14**, 928 (2023).
- [28] Y.-M. Xie, Y.-S. Lu, C.-X. Weng, X.-Y. Cao, Z.-Y. Jia, Y. Bao, Y. Wang, Y. Fu, H.-L. Yin, and Z.-B. Chen, Breaking the rate-loss bound of quantum key distribution with asynchronous two-photon interference, *PRX Quantum* **3**, 020315 (2022).
- [29] P. Zeng, H. Zhou, W. Wu, and X. Ma, Mode-pairing quantum key distribution, *Nat. Commun.* **13**, 3903 (2022).
- [30] Y.-M. Xie, C.-X. Weng, Y.-S. Lu, Y. Fu, Y. Wang, H.-L. Yin, and Z.-B. Chen, Scalable high-rate twin-field quantum key distribution networks without constraint of probability and intensity, *Phys. Rev. A* **107**, 042603 (2023).
- [31] Y.-M. Xie, J.-L. Bai, Y.-S. Lu, C.-X. Weng, H.-L. Yin, and Z.-B. Chen, Advantages of asynchronous measurement-device-independent quantum key distribution in intercity networks, *Phys. Rev. Applied* **19**, 054070 (2023).
- [32] I. V. Puthoor, R. Amiri, P. Wallden, M. Curty, and E. Andersson, Measurement-device-independent quantum digital signatures, *Phys. Rev. A* **94**, 022328 (2016).
- [33] T. Shang, Q. Lei, and J. Liu, Quantum random oracle model for quantum digital signature, *Phys. Rev. A* **94**, 042314 (2016).
- [34] M. Thornton, H. Scott, C. Croal, and N. Korolkova, Continuous-variable quantum digital signatures over insecure channels, *Phys. Rev. A* **99**, 032341 (2019).
- [35] Y.-S. Lu, X.-Y. Cao, C.-X. Weng, J. Gu, Y.-M. Xie, M.-G. Zhou, H.-L. Yin, and Z.-B. Chen, Efficient quantum digital signatures without symmetrization step, *Opt. Express* **29**, 10162 (2021).
- [36] C.-H. Zhang, X. Zhou, C.-M. Zhang, J. Li, and Q. Wang, Twin-field quantum digital signatures, *Opt. Lett.* **46**, 3757 (2021).
- [37] C.-X. Weng, Y.-S. Lu, R.-Q. Gao, Y.-M. Xie, J. Gu, C.-L. Li, B.-H. Li, H.-L. Yin, and Z.-B. Chen, Secure and practical multiparty quantum digital signatures, *Opt. Express* **29**, 27661 (2021).
- [38] J.-Q. Qin, C. Jiang, Y.-L. Yu, and X.-B. Wang, Quantum digital signatures with random pairing, *Phys. Rev. Applied* **17**, 044047 (2022).
- [39] R. J. Collins, R. Amiri, M. Fujiwara, T. Honjo, K. Shimizu, K. Tamaki, M. Takeoka, E. Andersson, G. S. Buller, and M. Sasaki, Experimental transmission of quantum digital signatures over 90 km of installed optical fiber using a differential phase shift quantum key distribution system, *Opt. Lett.* **41**, 4883 (2016).
- [40] H.-L. Yin, Y. Fu, H. Liu, Q.-J. Tang, J. Wang, L.-X. You, W.-J. Zhang, S.-J. Chen, Z. Wang, Q. Zhang, T.-Y. Chen, Z.-B. Chen, and J.-W. Pan, Experimental quantum digital signature over 102 km, *Phys. Rev. A* **95**, 032334 (2017).
- [41] H.-L. Yin, W.-L. Wang, Y.-L. Tang, Q. Zhao, H. Liu, X.-X. Sun, W.-J. Zhang, H. Li, I. V. Puthoor, L.-X. You, E. Andersson, Z. Wang, Y. Liu, X. Jiang, X. Ma, Q. Zhang, M. Curty, T.-Y. Chen, and J.-W. Pan, Experimental measurement-device-independent quantum digital signatures over a metropolitan network, *Phys. Rev. A* **95**, 042338 (2017).
- [42] G. Roberts, M. Lucamarini, Z. Yuan, J. Dynes, L. Comandar, A. Sharpe, A. Shields, M. Curty, I. Puthoor, and E. Andersson, Experimental measurement-device-independent quantum digital signatures, *Nat. Commun.* **8**, 1098 (2017).
- [43] C.-H. Zhang, X.-Y. Zhou, H.-J. Ding, C.-M. Zhang, G.-C. Guo, and Q. Wang, Proof-of-principle demonstration of passive decoy-state quantum digital signatures over 200 km, *Phys. Rev. Applied* **10**, 034033 (2018).
- [44] X.-B. An, H. Zhang, C.-M. Zhang, W. Chen, S. Wang, Z.-Q. Yin, Q. Wang, D.-Y. He, P.-L. Hao, S.-F. Liu, X.-Y. Zhou, G.-C. Guo, and Z.-F. Han, Practical quantum digital signature with a gigahertz bb84 quantum key distribution system, *Opt. Lett.* **44**, 139 (2019).
- [45] H.-J. Ding, J.-J. Chen, L. Ji, X.-Y. Zhou, C.-H. Zhang,

- C.-M. Zhang, and Q. Wang, 280-km experimental demonstration of a quantum digital signature with one decoy state, *Opt. Lett.* **45**, 1711 (2020).
- [46] S. Richter, M. Thornton, I. Khan, H. Scott, K. Jaksch, U. Vogl, B. Stiller, G. Leuchs, C. Marquardt, and N. Korolkova, Agile and versatile quantum communication: Signatures and secrets, *Phys. Rev. X* **11**, 011038 (2021).
- [47] Y. Pelet, I. V. Puthoor, N. Venkatachalam, S. Wengerovsky, M. Loncaric, S. P. Neumann, B. Liu, Z. Samec, M. Stipčević, R. Ursin, *et al.*, Unconditionally secure digital signatures implemented in an 8-user quantum network, *New J. Phys.* **24**, 093038 (2022).
- [48] H.-L. Yin, Y. Fu, C.-L. Li, C.-X. Weng, B.-H. Li, J. Gu, Y.-S. Lu, S. Huang, and Z.-B. Chen, Experimental quantum secure network with digital signatures and encryption, *Natl. Sci. Rev.* **10**, nwac228 (2023).
- [49] B.-H. Li, Y.-M. Xie, X.-Y. Cao, C.-L. Li, Y. Fu, H.-L. Yin, and Z.-B. Chen, One-time universal hashing quantum digital signatures without perfect keys, arXiv preprint arXiv:2301.01132 (2023).
- [50] S. L. Braunstein and S. Pirandola, Side-channel-free quantum key distribution, *Phys. Rev. Lett.* **108**, 130502 (2012).
- [51] K. Tamaki, M. Curty, G. Kato, H.-K. Lo, and K. Azuma, Loss-tolerant quantum cryptography with imperfect sources, *Phys. Rev. A* **90**, 052314 (2014).
- [52] F. Xu, K. Wei, S. Sajeed, S. Kaiser, S. Sun, Z. Tang, L. Qian, V. Makarov, and H.-K. Lo, Experimental quantum key distribution with source flaws, *Phys. Rev. A* **92**, 032305 (2015).
- [53] Z. Tang, K. Wei, O. Bedrova, L. Qian, and H.-K. Lo, Experimental measurement-device-independent quantum key distribution with imperfect sources, *Phys. Rev. A* **93**, 042308 (2016).
- [54] K.-i. Yoshino, M. Fujiwara, K. Nakata, T. Sumiya, T. Sasaki, M. Takeoka, M. Sasaki, A. Tajima, M. Koashi, and A. Tomita, Quantum key distribution with an efficient countermeasure against correlated intensity fluctuations in optical pulses, *npj Quantum Inf.* **4**, 8 (2018).
- [55] M. Pereira, M. Curty, and K. Tamaki, Quantum key distribution with flawed and leaky sources, *npj Quantum Inf.* **5**, 62 (2019).
- [56] A. Navarrete, M. Pereira, M. Curty, and K. Tamaki, Practical quantum key distribution that is secure against side channels, *Phys. Rev. Applied* **15**, 034072 (2021).
- [57] X.-B. Wang, X.-L. Hu, and Z.-W. Yu, Practical long-distance side-channel-free quantum key distribution, *Phys. Rev. Applied* **12**, 054034 (2019).
- [58] F. Xu, X. Ma, Q. Zhang, H.-K. Lo, and J.-W. Pan, Secure quantum key distribution with realistic devices, *Rev. Mod. Phys.* **92**, 025002 (2020).
- [59] M. Pereira, G. Kato, A. Mizutani, M. Curty, and K. Tamaki, Quantum key distribution with correlated sources, *Sci. Adv.* **6**, eaaz4487 (2020).
- [60] C. Zhang, X.-L. Hu, C. Jiang, J.-P. Chen, Y. Liu, W. Zhang, Z.-W. Yu, H. Li, L. You, Z. Wang, *et al.*, Experimental side-channel-secure quantum key distribution, *Phys. Rev. Lett.* **128**, 190503 (2022).
- [61] J. Gu, X.-Y. Cao, Y. Fu, Z.-W. He, Z.-J. Yin, H.-L. Yin, and Z.-B. Chen, Experimental measurement-device-independent type quantum key distribution with flawed and correlated sources, *Sci. Bull.* **67**, 2167 (2022).
- [62] R. König, R. Renner, and C. Schaffner, The operational meaning of min- and max-entropy, *IEEE Trans. Inf. Theory* **55**, 4337 (2009).
- [63] Amazon Web Services Customer Agreement, https://aws.amazon.com/agreement/?nc1=h_ls (2023).
- [64] M. Lucamarini, I. Choi, M. B. Ward, J. F. Dynes, Z. L. Yuan, and A. J. Shields, Practical security bounds against the trojan-horse attack in quantum key distribution, *Phys. Rev. X* **5**, 031030 (2015).
- [65] H. Krawczyk, LFSR-based hashing and authentication, in *Annual International Cryptology Conference* (1994) pp. 129–139.
- [66] H.-L. Yin, M.-G. Zhou, J. Gu, Y.-M. Xie, Y.-S. Lu, and Z.-B. Chen, Tight security bounds for decoy-state quantum key distribution, *Sci. Rep.* **10**, 14312 (2020).
- [67] S. Sun, Security of reference-frame-independent quantum key distribution with source flaws, *Phys. Rev. A* **104**, 022423 (2021).
- [68] K. Tamaki, H.-K. Lo, C.-H. F. Fung, and B. Qi, Erratum: Phase encoding schemes for measurement-device-independent quantum key distribution with basis-dependent flaw [Phys. Rev. A 85, 042307 (2012)], *Phys. Rev. A* **86**, 059903 (2012).
- [69] G. Kato, Concentration inequality using unconfirmed knowledge, arXiv preprint arXiv:2002.04357 (2020).
- [70] G. Brassard and L. Salvail, Secret-key reconciliation by public discussion, in *Advances in Cryptology—EUROCRYPT’93* (1994) pp. 410–423.
- [71] V. Shoup, On fast and provably secure message authentication based on universal hashing, in *Annual International Cryptology Conference (CRYPTO)* (Springer, 1996) pp. 313–328.
- [72] J. Massey, Shift-register synthesis and bch decoding, *IEEE Trans. Inf. Theory* **15**, 122 (1969).
- [73] W. Hoeffding, Probability inequalities for sums of bounded random variables, *The collected works of Wassily Hoeffding*, 409 (1994).

SUPPLEMENTARY MATERIALS

SECTION S1. IRREDUCIBLE POLYNOMIALS

Irreducible polynomials play an important role in hashing process. The linear feedback shift register (LFSR) Toeplitz hash function is decided by a randomly selected irreducible polynomial of order n in $\text{GF}(2)$ and an initial random bit string. Here we introduce the definition and criteria of irreducible polynomials, and solutions to randomly generating an irreducible polynomials in $\text{GF}(2)$.

A. Introduction to irreducible polynomials in $\text{GF}(2)$
All polynomials in $\text{GF}(2)$, with coefficients only being ‘0’ or ‘1’, composite a ring, where all calculation obeys the rules in $\text{GF}(2)$. A polynomial in $\text{GF}(2)$ is irreducible means that no polynomials can divide it except the identity element ‘1’ and itself, under calculation rules in $\text{GF}(2)$. Denote a polynomial of order n in $\text{GF}(2)$ as $p(x)$. There is another necessary and sufficient condition for $p(x)$ being irreducible that

$$\begin{cases} x^{2^n} \equiv x \pmod{p(x)} \\ \text{gcf}(x^{2^{\frac{n}{d}}} - x, p(x)) = 1 \end{cases}, \quad (\text{S1})$$

for all d that is prime factor of n , where $\text{gcf}(f(x), g(x))$ represents the greatest common factor of $f(x)$ and $g(x)$.

B. Generating an irreducible polynomials in $\text{GF}(2)$ in random

The condition above offers a way to testing the irreducibility of a polynomial. Trivially, there is a solution to randomly generating an irreducible polynomials in $\text{GF}(2)$. One can directly generate a polynomial through random numbers and test for its irreducibility by repeating this step until a polynomial passes the test. We denote this solution as the test algorithm. When $n = 2^k$, parameter d can only be 2, and thus the test algorithm is quite efficient by utilizing fast modular composition algorithm and n extended Euclidean algorithm. [48] However, under other scenarios the test may consume too much computational resources and also require too many random numbers. In the following we introduce another approach with higher efficiency [71], denoted as the generating algorithm. This solution requires presetting an irreducible polynomial of order n , defining the extension field $\text{GF}(2^n)$. Another random number decides a random element in $\text{GF}(2^n)$. The minimal polynomial of this random element in this field $\text{GF}(2^n)$ must be irreducible. Thus, by computing the minimal polynomial of this element one can get a random irreducible polynomial. An efficient process to obtain the minimal polynomial is shown below.

First, denote the initial irreducible polynomial as $f(x)$ and the polynomial generated by random element as $g(x)$. Then calculate the sequence $a_0 = g_0(0)$, $a_1 = g_1(0)$, ..., $a_{2n-1} = g_{2n-1}(0)$ in turn, where $g_i(x) = g^i(x) \pmod{f(x)}$. This sequence of $2n$ elements can fully determine the minimal polynomial of $g(x)$, i.e., the monic polynomial $h(x)$ of least order such that $h(g(x)) = 0 \pmod{f(x)}$,

which can be efficiently computed by Berlekamp-Massey algorithm [72]. The result, i.e., the minimal polynomial of $g(x)$, will be the random irreducible polynomial we generate. The probability of this polynomial to be n -order is more than $1 - 2^{-n/2}$. If the order is less than n , we can just choose another random number and repeat the process.

Here, we give a demonstration of the generating algorithm for order $n = 8$ as an example. First, preset the initial irreducible polynomial $f(x) = x^8 + x^7 + x^6 + x + 1$, and input a random bit string (01111100), corresponding to $g(x) = x^6 + x^5 + x^4 + x^3 + x^2$. Then calculate $g_2(x) = g^2(x) \pmod{f(x)} = x^6 + x^5 + x^4 + x^3 + x^2$, $g_3(x) = g^3(x) \pmod{f(x)} = x^4 + x$, ..., $g_{15}(x) = g^{15}(x) \pmod{f(x)} = x^7 + x^6 + x^5 + x^3 + x^2 + x$. Then we can obtain a sequence s with $s(0) = g_0(0) = 1$, $s(1) = g_1(0) = 0$, $s(2) = g_2(0) = 0$, ..., $s(15) = g_{15}(0) = 0$, i.e., $s = (100000101011110)$. Finally, input s into Berlekamp-Massey algorithm with $\text{GF}(2)$, and we can obtain the output (101111011), corresponding to the generated random irreducible polynomial $h(x) = x^8 + x^6 + x^5 + x^4 + x^3 + x + 1$.

The test algorithm can only be effectively accelerated when the order $n = 2^k$ [48]. The generating algorithm will be more efficient than the test algorithm even under this circumstance. We simulate the time consumption of the generating algorithm and the test algorithm, with $n = 256$ as an example. The results shows that it takes 1016.57 seconds to generate twenty random irreducible polynomials through the test algorithm, and only 133.4 seconds if using the generating algorithm. The time consumption of the test algorithm will be longer if $n \neq 2^k$. It shows that the generating algorithm is quite efficient.

SECTION S2. CHARACTERIZATION OF SOURCE FLAWS

As a MDI type protocol, our protocol has no assumptions on the middle node, which means that we only need to consider the imperfections at the source. Since KGP in our scheme is based on four-phase MDI QKD, our protocol inherits its advantages and the way to characterize the source flaws. Here, we show how to get the parameters of the source flaws in this section. We consider the worst case scenario here and the structure and devices used in this setup are identical to those used in the plug-and-play system for key generation, with the only difference being the removal of extra attenuation. The quality of the radio frequency modulation signals for the modulation and synchronization of the system has a direct impact on the results of characterization. All radio frequency signals we used were produced by an arbitrary waveform generator with a sampling rate of 2.5 G · Sa/s (Tabor Electronics, P2588B). Note that random numbers are generated by a home-made quantum random number generator and the cycle length is 10000. The electrical drivers we used are DR-VE-10-MO (iXblue), and the ultra-low voltage

PMs are PM-5S5-10-PFA-UV (Eospace). During our implementation, we conducted three rounds of KGP, and we also performed three rounds of calibrations of the source, whose results showed minor differences.

A. State preparation flaws

State preparation flaws results from imperfect intensity modulation and phase modulation and the practical state can be written as [61]:

$$\begin{aligned} |\Psi_X^*\rangle &= \frac{1}{\sqrt{2}} \left(|0_X\rangle |\alpha_0\rangle + |1_X\rangle |-e^{i(\pi+\delta_1)}\alpha_1\rangle \right), \\ |\Psi_Y^*\rangle &= \frac{1}{\sqrt{2}} \left(|1_Y\rangle |ie^{i(\pi/2+\delta_2)}\alpha_2\rangle + |0_Y\rangle |-ie^{i(3\pi/2+\delta_3)}\alpha_3\rangle \right). \end{aligned} \quad (S2)$$

We define δ_i as the difference between the actual phase and the expected phase, $i \in \{1, 2, 3\}$. In our scheme, there is no need for multi-intensity modulation and we only need to consider imperfect phase modulations, which is named phase shift. Another point is optical power fluctuation, caused by the volatility of the path attenuation and the light source itself. We show how to quantify specific parameters through experiments in the following.

(i) Optical power fluctuation

During our implementation, the intensity of pulses is a constant under a specific channel loss. Nevertheless, due to the inherent fluctuations of the light source and path variations, the intensity of the light is not a constant. $|\alpha'|^2$ represents the realistic intensity modulation of coherent pulses. The deviation ratio can be denoted by $\xi' = ||\alpha'|^2 - |\alpha|^2| / |\alpha|^2$ and ξ is the maximum value of ξ' . With no intensity modulation, we can quantify this parameter by measuring the optical power fluctuations. We recorded the values of the optical power meter (Joinwit, JW8103D) every 500 ms for 600 seconds.

We separated the optical power fluctuations into two parts: the intrinsic fluctuation of the light source and the path fluctuation. Note that the added attenuation also causes fluctuation and we distributed the attenuation into two measurement processes to ensure that the values of optical power are not only greater than the power meter's minimum detectable value, but also the pulse intensity after the total attenuation is lower than the minimum value used in the experiment. We measured the fluctuation of the light source by directly connecting the light source to a power meter after introducing an additional attenuation of approximately 40 dB, where the attenuation values slightly vary among the three groups. While for path fluctuation, we directly disconnected the optical loop and connected a power meter at the output port of a participant to measure the optical power fluctuations after the pulses passed through the entire Sagnac loop. Different attenuations were also introduced to facilitate their display in Fig. 4. The maximum values of ξ

in different pairs of participants (Merchant - TP₁, Merchant - Client and Merchant - TP₂) are 0.79%, 0.69% and 0.62%.

(ii) Phase shift

From Eq. S2, we can know imperfect phase modulation can be quantified by $\delta = \max\{\bar{\delta}_1, \bar{\delta}_2, \bar{\delta}_3\}$. Similar to Ref. [52, 61], the structure and parameters of the measurement system are the same as the plug-and-play system. During implementation, Merchant performs phase modulation randomly while Client sets his PM at a fixed phase 0. Two pulse trains interfere at Eve's BS and the interference results are detected by single-photon detectors. Here, the random number resource used by Merchant is the same as that used in the KGP and the intensity of pulses is set as 0.001. We ran the system for 100 seconds and recorded the corresponding results. We employed Hoeffding's inequality [73] to get the upper bound of δ_ϕ (Eq. S3), where η_{d_i} is the detection efficiency of detectors and $\bar{D}_{i,\phi} = D_{i,\phi} + \sqrt{D_{i,\phi}/2 \ln(1/\varepsilon)}$ ($i \in \{1, 2\}$) and $\varepsilon = 10^{-10}$ is the failure probability. For $\phi \in [0, \pi]$, we have $\phi_0 = \phi$, and for $\phi \in (\pi, 2\pi]$, $\phi_0 = \phi - \pi$. The detailed detection results and their upper bounds of phase shift are presented in Table III. Consequently, the values of δ are 0.038, 0.035 and 0.035, respectively.

B. Side channels caused by polarization

Various kinds of side channels caused by mode dependencies exist in a QKD system, through which the eavesdropper can distinguish the states. In our scheme, we only consider the polarization space as the side-channel space and the coherent states can be written as

$$\begin{aligned} |\alpha'_0\rangle &= \cos\theta_0 |\alpha_0\rangle_H + \sin\theta_0 |\alpha_0\rangle_V, \\ |\alpha'_1\rangle &= \cos\theta_1 |-e^{i(\pi/2+\delta_1)}\alpha_1\rangle_H + \sin\theta_1 |-e^{i(\pi/2+\delta_1)}\alpha_1\rangle_V, \\ |\alpha'_2\rangle &= \cos\theta_2 |ie^{i(\pi+\delta_2)}\alpha_2\rangle_H + \sin\theta_2 |ie^{i(\pi+\delta_2)}\alpha_2\rangle_V, \\ |\alpha'_3\rangle &= \cos\theta_3 |-ie^{i(3\pi/2+\delta_3)}\alpha_3\rangle_H + \sin\theta_3 |-ie^{i(3\pi/2+\delta_3)}\alpha_3\rangle_V, \end{aligned} \quad (S4)$$

where H and V represent two orthogonal states. As we consider the worst scenario where the maximum deviation θ applies to all states here, we can assume $\theta_i = \theta$ ($i \in \{0, 1, 2, 3\}$). Thus, the states with side channels and state preparation flaws can be expressed as

$$\begin{aligned} |\Psi'_X\rangle &= \frac{1}{\sqrt{2}} (|0_X\rangle |\alpha'_0\rangle + |1_X\rangle |\alpha'_1\rangle), \\ |\Psi'_Y\rangle &= \frac{1}{\sqrt{2}} (|1_Y\rangle |\alpha'_2\rangle + |0_Y\rangle |\alpha'_3\rangle). \end{aligned} \quad (S5)$$

For quantification, we only need to get the maximum deviation of θ . As we used the horizontal states to form secret key, the extinction ratio of polarization in the system can be represented by $\tan\theta$. The extinction ratio of polarization of the sent pulses is the ratio of the optical power along the fast-axis to the slow-axis. To obtain this ratio, a polarization beam splitter (PBS) is placed at a

$$\bar{\delta}_\phi = \max \left\{ \left| \phi_0 - 2\arctan \sqrt{\frac{(\bar{D}_{2,\phi} - \underline{D}_{2,0})/\eta_{d_2}}{(\underline{D}_{1,\phi} - \bar{D}_{2,0})/\eta_{d_1}}} \right|, \left| \phi_0 - 2\arctan \sqrt{\frac{(\underline{D}_{2,\phi} - \bar{D}_{2,0})/\eta_{d_2}}{(\bar{D}_{1,\phi} - \underline{D}_{2,0})/\eta_{d_1}}} \right| \right\}. \quad (S3)$$

participant's site and we measured the optical power at both ports of the PBS using a power meter. The measurements were taken once every 500 ms and were carried out for 600 seconds. As shown in Fig. 5, the orange points mean the extinction ratio of polarization. The maximum values of the extinction ratio of pulse polarization in three rounds of KGP are -29.2 dB, -30 dB and -29.8 dB, and thus the values of $\tan \theta$ are $10^{-2.92}$, 10^{-3} and $10^{-2.98}$, respectively.

C. Trojan horse attacks

Here, we consider a type of THA where an eavesdropper, Eve, injects strong light into the optical devices at the participants' sites and obtains modulation information by measuring the reflected light. To model this type of attack, the pulse state $|\xi\rangle_E$ held by Eve can be expressed as $e^{-\mu/2}|\alpha_Z\rangle + \sqrt{1-e^{-\mu}}|\beta_Z\rangle$, where $T \in \{0_x, 0_y, 1_x, 1_y\}$ represents the bit value and basis selection, and μ is the intensity of Eve's back-reflected pulses [55]. In the worst case scenario, where $\langle \xi_T | \xi_{T'} \rangle_E = 0$, and considering the state preparation flaws and side-channel effects, the states can be expressed as

$$\begin{aligned} |\Psi_X''\rangle &= \frac{1}{\sqrt{2}} (|0_X\rangle |\alpha'_0\rangle |\zeta_{0X}\rangle_E + |1_X\rangle |\alpha'_1\rangle |\zeta_{1X}\rangle_E), \\ |\Psi_Y''\rangle &= \frac{1}{\sqrt{2}} (|1_Y\rangle |\alpha'_2\rangle |\zeta_{1Y}\rangle_E + |0_Y\rangle |\alpha'_3\rangle |\zeta_{0Y}\rangle_E). \end{aligned} \quad (S6)$$

Note that the scheme with two independent users can resist THAs. However, the plug-and-play system is vulnerable to such attacks, since the pulses are generated by a third party. We set $\mu = 10^{-7}$ [64] to illustrate the robustness of our scheme to such attacks.

D. Pattern effect

Security analyses of quantum protocols tend to be based on the assumption of independent distributed pulses. However, pulse correlation resulting from band-limited devices is almost impossible to avoid in practical systems. In this way, as the system frequency increases, the value of ψ will rapidly increase, significantly influencing the signature rate. Encoding logic bits with phase information removes the requirements of vacuum state preparation in our protocol, which makes our scheme free from intensity correlation [54], and the pulse correlation, also called pattern effect, caused by phase modulation

can be observed in our implementation. According to Ref. [59, 61], the state can be written as

$$\begin{aligned} |\Psi_X\rangle &= \sqrt{1-\epsilon}|\Psi_X''\rangle + \sqrt{\epsilon}|\Psi_X''^\perp\rangle, \\ |\Psi_Y\rangle &= \sqrt{1-\epsilon}|\Psi_Y''\rangle + \sqrt{\epsilon}|\Psi_Y''^\perp\rangle, \end{aligned} \quad (S7)$$

where ϵ is the parameter characterizing the pulse correlation and $|\Psi_Z''^\perp\rangle$ ($Z \in \{X, Y\}$) means the state considering pulse correlation and is orthogonal to $|\Psi_Z''\rangle$. We consider the worst case where $\langle \Psi_X''^\perp | \Psi_Y''^\perp \rangle = 0$. Here we only consider the pattern effects limited to the adjacent pulses for simplicity and we define the maximum phase deviation ψ . Assume we prepare a state $|\alpha\rangle$ and the practical state is $|e^{i\psi}\alpha\rangle$. Obviously, $\langle \alpha | e^{i\psi}\alpha \rangle = e^{(e^{i\psi}-1)|\alpha|^2}$. According to Eq. S7, $\langle \alpha | e^{i\psi}\alpha \rangle = \sqrt{1-\epsilon}$. Consequently, we can obtain the relation $\epsilon = 1 - e^{|\alpha|^2(2\cos\psi-2)}$. For state $|\alpha\rangle$ after phase modulation ($\theta \in \{0, \pi/2, \pi, 3\pi/2\}$), $|\alpha'\rangle = |e^{i(\psi+\theta)}\alpha\rangle$. Thus the interference results are $\frac{e^{i\psi}\pm 1}{\sqrt{2}}|\alpha\rangle$. Consequently, the deviation of intensity in the interference results is $\sin\psi$. This is reflected in the experimental results as the proportion of the deviation of the detection counts for different patterns from their mean values.

We specifically focus on the correlation between adjacent pulses, resulting in a total of sixteen possible patterns. The Client's PM is set to an unmodulated phase 0 and Merchant generates each pattern with an equal probability. The pulses interfered at Eve's BS, and the results were measured by detectors D_1 and D_2 . To reduce the impact of statistical fluctuations and dark counts, we calculated the deviation values of phase 0 and $\pi/2$ by D_1 's detection results while the deviation values of phase π and $3\pi/2$ are given by D_2 's detection results. As presented in Table IV, the maximum values of $\sin\psi$ are 5.58×10^{-3} , 5.89×10^{-3} and 6.91×10^{-3} . Thus, we can get ψ , which are equal to corresponding $\sin\psi$ values.

SECTION S3. EXPERIMENTAL DATA

The calibrated efficiencies of different optical elements in Eve's site are listed in Table V. The detection results during implementation are summarized in Table VI, including the number of all detection events n , the number of detection events under X basis n_x , the number of detection events under Y basis n_y and the number of detection events under different added phases. The number of detection events under different phases is labelled as "Detected MC", where "M" ("C") means an M (C) phase was added on the pulses by Merchant (Client) and detected by D_i , $i \in \{1, 2\}$.

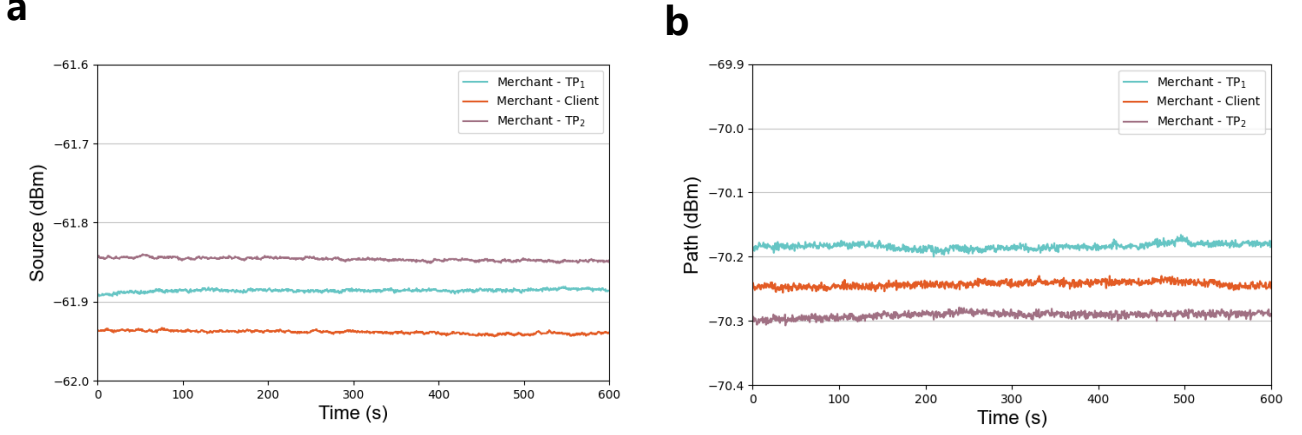


FIG. 4. **Optical power fluctuation.** **a.** Source fluctuation. **b.** Path fluctuation. The maximum fluctuation of the laser source within 100 seconds was measured to be 0.009 dBm, 0.008 dBm, and 0.008 dBm, respectively. For the path fluctuation, the corresponding values were 0.025 dBm, 0.022 dBm, and 0.019 dBm. As a result, the maximum optical power fluctuations within the 100-second duration were found to be smaller than 0.79% (0.034 dBm), 0.69% (0.03 dBm), and 0.62% (0.027 dBm), respectively.

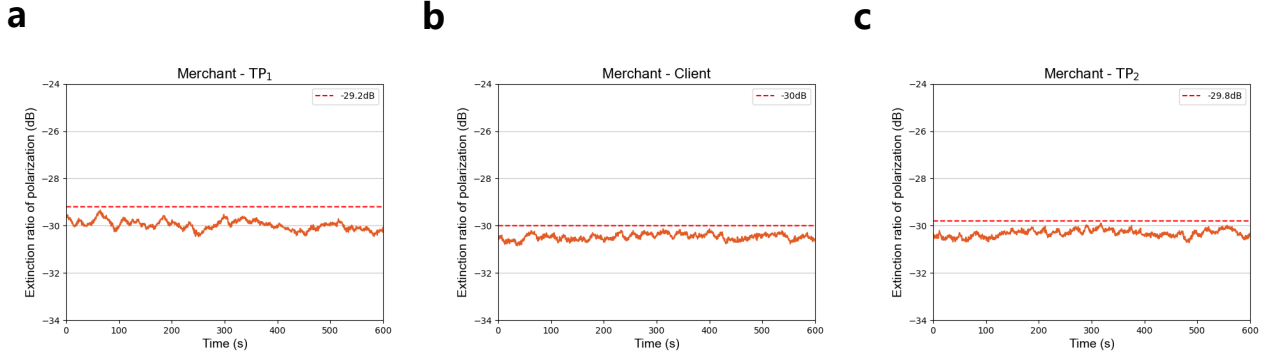


FIG. 5. **The extinction ratios of polarization measured over time in three systems.** The obtained values consistently remained below -29.2 dB, -30 dB, and -29.8 dB during the ten-minute duration.

TABLE III. **Upper bounds of phase shifts under different phases between different pair of participants.** $D_{1,\phi}$ and $D_{2,\phi}$ are the number of clicks detected by D_1 and D_2 under different phases ϕ ($\phi \in \{0, \pi/2, \pi, 3\pi/2\}$) and their upper bounds are denoted by $\bar{\delta}_\phi$.

ϕ	Merchant - TP ₁			Merchant - Client			Merchant - TP ₂		
	$D_{1,\phi}$	$D_{2,\phi}$	$\bar{\delta}_\phi$	$D_{1,\phi}$	$D_{2,\phi}$	$\bar{\delta}_\phi$	$D_{1,\phi}$	$D_{2,\phi}$	$\bar{\delta}_\phi$
0	5399578	1386	-	5399006	1927	-	5398064	1475	-
$\pi/2$	335935	384598	0.013	337584	383687	0.016	336621	385404	0.013
π	2954	6130443	0.038	3176	6135875	0.035	2817	6131470	0.035
$3\pi/2$	309240	340297	0.033	308194	341223	0.030	308961	339748	0.033

TABLE IV. **Detection data for pattern effect.** We recorded the number of clicks of pulses with different phases for each of the sixteen patterns n_{pa} , from which the value of $\sin \psi$ can be obtained. We also present $\sin \bar{\psi}$ (the maximum deviation value from the average value of different phases) in the table.

Pattern	Merchant - TP ₁		Merchant - Client		Merchant - TP ₂	
	n_{pa}	$\sin \bar{\psi}$	n_{pa}	$\sin \bar{\psi}$	n_{pa}	$\sin \bar{\psi}$
$S_1 \rightarrow S_1$	375878		375953		375153	
$S_2 \rightarrow S_1$	374914	2.29×10^{-3}	376614	1.50×10^{-3}	374603	4.69×10^{-3}
$S_3 \rightarrow S_1$	375931		375953		374532	
$S_4 \rightarrow S_1$	376382		375673		377112	
$S_1 \rightarrow S_2$	188037		188555		187043	
$S_2 \rightarrow S_2$	187634	3.98×10^{-3}	188907	3.28×10^{-3}	188196	6.91×10^{-3}
$S_3 \rightarrow S_2$	189045		188349		189378	
$S_4 \rightarrow S_2$	188469		187780		188763	
$S_1 \rightarrow S_3$	430459		429037		429414	
$S_2 \rightarrow S_3$	429219	3.14×10^{-3}	428304	1.52×10^{-3}	428170	2.52×10^{-3}
$S_3 \rightarrow S_3$	428810		428710		427898	
$S_4 \rightarrow S_3$	427953		429951		427851	
$S_1 \rightarrow S_4$	214274		211948		213956	
$S_2 \rightarrow S_4$	212405	5.58×10^{-3}	214372	5.89×10^{-3}	211503	6.59×10^{-3}
$S_3 \rightarrow S_4$	213151		214151		211880	
$S_4 \rightarrow S_4$	214556		211993		214285	

TABLE V. **The efficiencies of optical elements.** The efficiency of Cir 2→3 means the total efficiency of pulses from circulator's port 2 to port 3. The efficiency of BS-1 means the efficiency of pulses to port 1. The same applies to BS-2.

Optical element	Efficiency
Cir 2→3	86.9%
BS-1	85.5%
BS-2	86.0%
PC ₁	96.2%
PC ₂	95.4%

TABLE VI. Detailed experimental data under different channel losses.

Channel loss	15 dB		20 dB		25 dB	
n	17189504		5463449		1707401	
n_x	13919127		4424989		1382365	
n_y	189603		60019		18850	
Detector	D1	D2	D1	D2	D1	D2
Detected 00	3298168	1733	1050551	523	328219	184
Detected 0π	4570	3685584	1571	1171773	486	366036
Detected $\pi 0$	5660	3734246	1761	1186466	463	371271
Detected $\pi \pi$	3186629	2537	1011575	769	315436	270
Detected $\frac{\pi}{2} \frac{\pi}{2}$	34766	26	10931	7	3425	1
Detected $\frac{\pi}{2} \frac{3\pi}{2}$	22	59559	10	18708	6	5939
Detected $\frac{3\pi}{2} \frac{\pi}{2}$	43	53998	11	17177	6	5255
Detected $\frac{3\pi}{2} \frac{3\pi}{2}$	41141	48	13165	10	4212	6